Physicochem. Probl. Miner. Process., 60(1), 2024, 185763

http://www.journalssystem.com/ppmp

Physicochemical Problems of Mineral Processing

ISSN 1643-1049

Adsorption and desorption characteristics of rare earth ions on halloysite surfaces

Qibang Long [1,2,3], Huashan Yan [1,2,3], Xiaowen Zhou [2,3], Sen Qiu [4], Tingsheng Qiu [2,3]

[1] 1 Jiangxi Provincial Key Laboratory for Simulation and Modelling of Particulate Systems, Jiangxi University of Science and Technology, Nanchang 330013, Jiangxi Province, P.R. China

[2] College of Resource and Environmental Engineering, Jiangxi University of Science and Technology, Ganzhou 341000, Jiangxi Province, P.R. China

[3] Key Laboratory of Green Development and Utilization of Strategic Rare Metal Mineral Resources (Jiangxi University of Science and Technology), Ministry of Education, Ganzhou 341000, Jiangxi Province, P.R. China

[4] College of Rare Earth and New Materials Engineering, Gannan University of Science and Technology, Ganzhou 341000, Jiangxi Province, P.R. China

Corresponding authors: 9120190062@jxust.edu.cn (H. S. Yan), 9120090029@jxust.edu.cn (X. W. Zhou)

Abstract: Rare earths (REs) are primarily adsorbed in ionic form on the surface of clay minerals such as halloysite in ionic rare earth ores. As a result, understanding the adsorption and desorption behaviors of RE ions on the surface of the halloysite may contribute to clarifying the mineralization process of ionic rare earth ores and provide a theoretical framework for the optimization of the extraction process. The adsorption and desorption characteristics of light (Nd^{3+}), medium (Eu^{3+}), and heavy (Lu^{3+}) RE ions on the surface of halloysite-10 Å were comprehensively examined in this study. Because REs are more inclined to form an outer layer and inner layer adsorption when halloysite is protonated and deprotonated with the range of pH, respectively, pH has a significant impact on how halloysite adsorbs and desorbs. The experiment findings indicate that RE concentration, duration, and pH all increased the adsorption capacity of light, medium, and heavy REEs, and exhibited some selectivity for heavy REEs. Nd^{3+}, Eu^{3+} and Lu^{3+} ions adsorption processes on the surface of Halloysite-10 Å are consistent with the Langmuir isothermal adsorption model and pseudo-second-order kinetic equations. The desorption efficiency of Lu^{3+} decreases dramatically with increasing pH due to hydrolysis and more inner layer adsorption than that of Nd^{3+} and Eu^{3+}.

***Keywords*:** ionic rare earth ores, halloysite-10 Å, adsorption, desorption

1. Introduction

The term "rare earth metals" refers to a group of seventeen chemically related elements, which include the fifteen lanthanides found in positions 57 through 71 of the periodic table, as well as Sc and Y. They can be broadly categorized into three groups (with the exception of Pm and Sc): (1) light rare earth elements: La, Ce, Pr, Nd. (2) medium rare earth elements: Sm, Eu, Gd. (3) heavy rare earth elements: Tb, Dy, Ho, Er, Tm, Yb, Lu, and Y (Chi and Tian, 2006; Xiao et al., 2016). Owing to the numerous applications of rare earth elements in a range of industries, such as ceramic pigments (Liu et al., 2007), luminescent materials (Xie and Zhang, 2012), agriculture (Duan et al., 2014), permanent magnetic materials, iron and steel metallurgy (Ma, 2000), etc., rare earth elements are currently the subject of international competition and are regarded as one of China's most significant and strategically key metal mineral resources (Zhai et al., 2019). The main forms of rare earths in minerals include: the water-soluble phase, ionic phase, colloidal sedimentary phase, and mineral phase, of which the ionic phase rare earths are found in ion adsorption rare earth ores, whose original ore grade is low, but rare earths are complete of partition, low radioactivity, easy to mine, and are the main source of medium and heavy rare earths in the world. (Chi et al., 2012; Wang et al., 2021; Chen et al., 2022).

In warm and humid environments, rare earth ions released from the dissolution of rare earth-containing minerals (cerium fluorocarbon, cerium lanthanum spodumene, etc.) under a variety of

DOI: 10.37190/ppmp/185763

physical, chemical, and biological weathering continue to migrate along with the rain or groundwater, and are ultimately enriched to the surface of clay minerals, such as halloysite, as hydrated or hydroxyl-hydrated cations after a protracted period of the adsorption-desorption-migration process (Huang, 2006; Liang et al., 2022; Xu et al., 2017). Rare earth ions can be exchange leached from the clay surface into solution by using active cations (e.g., NH^{+4}, Mg^{2+}, Na^{+}, K^{+}, Fe^{2+}, Mn^{2+}) (Sun et al., 2017; Moldoveanu and Papangelakis, 2013; Xiao et al., 2015; Xiao et al., 2016(b); Xiao et al., 2018). Halloysite is a clay mineral formed via weathering that frequently co-occurs in weathering crusts with kaolinite, alumina trihydrate, and hydrous aluminum quartz (Han et al., 2011) and is most frequently seen as a dense clump or soil shape (Gao et al., 2018). It is a 1:1 type of silicate mineral with a structural unit layer made up of aluminium-oxygen octahedral sheets on the inner surface and silica-oxygen tetrahedral sheets on the outer surface (Jin et al., 2021). The amount of the clay mineral halloysite in weathered crust leach type rare earth ore is highest, followed by illite, kaolinite, and montmorillonite (Chi and Tian, 2007). Halloysite displays a variety of morphological features as a result of the regional variations, including: tubular, flaky, spherical, discoidal, and others (Niu et al., 2014). Halloysite can be further divided into 10 Å-halloysite, 7 Å-halloysite, and x Å-halloysite (x stands for (001) bottom spacing) depending on the discrepancy in hydration degree (Niu et al., 2014).

Coppin et al. (2002) implemented lanthanide adsorption experiments using montmorillonite and kaolinite at various pH levels and ionic strengths. The results suggested that the lanthanide adsorption coefficients were highly stable at low ionic strengths, while they increased with increasing pH at high ionic strengths. Gao et al. (2018) performed physical phase characterization analyses and adsorption modeling studies on kaolinite and halloysite-7 Å and discovered that when K^{+} is present in the system, halloysite preferentially adsorbs light REEs. Zhou et al. (2022) tested the adsorption-desorption of a single RE ion (Eu^{3+}) on kaolinite and halloysite (7 Å), they discovered that the adsorption behavior of Eu^{3+} on halloysite was more significantly affected by pH, with the adsorption capacity increasing by 53.55% from 3.38 mg/g (pH=4) to 5.19 mg/g (pH=6), However, under the same circumstances, kaolinite only saw a 13.76% increase in adsorption, and both clay minerals experienced an increase in desorption efficiency as NH^{+4} concentration increased. Qiu et al. (2022b) systematically examined the adsorption and desorption properties of halloysite and illite from numerous perspectives, including pH, contact time, and leaching agent concentration, they discovered that the adsorption capacity gradually increased with increasing pH (equilibrium was reached at pH=4), while the desorption efficiency gradually decreased, and that the majority of the RE ions adsorption (~95%) and desorption (~92%) could be finished essentially in 5 minutes. Li et al. (2016) discovered that halloysite-10 Å dominated the minerals in the Xishuangbanna deposit in Yunnan. Halloysite-10 Å can be totally dehydrated at a temperature of 100 °C to produce halloysite-7 Å, and halloysite can be heated to a specific point to increase its surface activity. Furthermore, research has demonstrated that the drying temperature, relative humidity, and sample source all affect how much halloysite-10 Å has dehydrated (Joussein et al., 2005). Numerous experimental research studies have been conducted on halloysite, however, the majority of them focus on halloysite-7 Å. There hasn't been a thorough investigation of the RE ion adsorption and desorption behavior on the surface of halloysite-10 Å. Studying the adsorption and desorption characteristics of halloysite-10 Å is necessary to achieve efficient leaching of rare earths in various clay minerals, optimize the extraction process, and reveal the adsorption mechanism and desorption variability of rare earth ions in various clay minerals.

The present work carefully examined and contrasted the effects of various pH values, time intervals, and concentrations on the adsorption and desorption of light (Nd^{3+}), medium (Eu^{3+}), and heavy (Lu^{3+}) RE ions on the surface of halloysite-10 Å. Powder X-ray Diffraction (XRD), Scanning Electron Microscopy (SEM) and Energy Dispersive Spectroscopy (EDS), and Zeta potential were used to describe the surface characteristics of halloysite-10 Å.

2. Materials and methods

2.1. Materials

The finely grained Halloysite-10 Å, obtained from Shanlin Stone Language Minerals Co., is the mineral that was employed in this study. All chemicals used were of analytical grade and included neodymium chloride (99.9%), europium chloride (99.9%), lutetium chloride (≥99.99%), as well as ammonium sulfate, hydrochloric acid, sulfuric acid, and sodium hydroxide.

2.2. Characterization method

Halloysite-10 Å was examined using XRD to determine its physical phase. The following were the relevant working conditions set: Cu Kα1 rays (\lambda=1.5406\ Å) with a diffraction angle of between 5° and 80° (2\theta), a working voltage of 40 V, and a working current of 40 mA were utilized.

In the test, the surface micro-zone morphology of the materials was observed using secondary electron imaging at an accelerating voltage of 20.0 KV, a working distance of 8.5 mm, and magnifications of 30,000 and 100,000 times. The scanning electron microscope (SEM) equipment utilized was the FEI-MLA650F. To determine how the elements were distributed on the mineral surface, the adsorbed samples were subjected to an energy dispersive spectroscopy (EDS) analysis.

Aqueous solutions with pH values of 3.0, 4.09, 5.05, 5.95, 6.94, 7.99, 9.04, 9.98, and 11.0, respectively, were mixed with 0.8 g of halloysite-10 Å to evaluate the pH buffering capabilities of halloysite-10 Å. The mixture was then placed in conical flasks and allowed to react for 60 minutes in a thermostatic water bath shaker. The halloysite samples have relatively tiny particle sizes, making direct filtering ineffective. As a result, the suspension must be moved to a centrifuge tube. The aqueous phase was then separated by centrifugation at a relative centrifugal force of 3130 ×g for 2 minutes, the filtrate was obtained by filtration using a microfiltration membrane, and the filtrate's pH value was measured using a pH meter and recorded.

2.3. Adsorption experiments

The molar ratio of Nd^{3+}, Eu^{3+}, and Lu^{3+} was 1:1:1, $NdCl_3$, $EuCl_3$, and $LuCl_3$ were combined to form mixed RE solutions with a 0.5 mmol/L concentration for each REE. For all conditional adsorption studies, the halloysite-10 Å/liquid ratio was maintained at 1:25. To reach the adsorption equilibrium, 0.5 g of halloysite-10 Å and 12.5 mL of RE solution at pH=5.25 were progressively put into conical flasks, covered with cling film, and then oscillated for 4 hours at 25 °C (±3℃) in a thermostatic water-bath oscillator. Following the cessation of oscillation, the solution was transferred to a centrifuge tube for centrifugation and filtration. An inductively coupled plasma optical emission spectrometry (ICP-OES) device was then used to measure the concentrations of Nd^{3+}, Eu^{3+}, and Lu^{3+} in the filtrate. Each experiment was repeated thrice. Equation (1) was applied to determine the equilibrium adsorption capacities (Q_e):

$$Q_e = \frac{(C_0 - C_e) \times V}{M} \quad (1)$$

where V is the volume of the solution (L), M is the mass of halloysite-10 Å (g), C0 is the concentration of rare earth in the solution before adsorption (mg/L) and Ce is the concentration of rare earth in the supernatant following adsorption equilibrium (mg/L).

2.3.1. Isothermal adsorption experiments

By applying 0.1 mol/L HCl and 0.1 mol/L NaOH to alter the solution pH to 2.01, 2.85, 4.02, 4.76, and 5.76 in accordance with the mentioned above adsorption experiment procedures, the effects of varying pH on the adsorption of Nd^{3+}, Eu^{3+}, and Lu^{3+} on halloysite-10 Å were examined. Then, all desorption experiments were performed using a $(NH_4)_2SO_4$ solution with a pH of 4.76 and a liquid-solid ratio of 25:1.

According to the above adsorption experiment steps, mixed solutions of Nd^{3+}, Eu^{3+}, and Lu^{3+} with concentrations ranging from 0.1 to 0.6 mmol/L were used to examine the impact of various RE concentrations on the adsorption experiment. The experimental data were then fitted using the Langmuir and Freundlich isothermal adsorption model.

2.3.2. Adsorption kinetics experiments

To study the effects of different contact times on the adsorption of Nd^{3+}, Eu^{3+}, and Lu^{3+} by halloysite-10 Å, 0.5 g of halloysite-10 Å was mixed with a rare earth solution of Nd^{3+}, Eu^{3+}, and Lu^{3+} at a concentration of 0.5 mmol/L, pH=5.25, and shaken in a thermostatic water-bath oscillator for 1, 3, 5, 10, 20, 30, 60, 120, 180, and 240 minutes, respectively. Equation (2) was used to determine the adsorption rates of Nd^{3+}, Eu^{3+}, and Lu^{3+}. Additionally, the experimental data were fit using the pseudo-first-order and pseudo-second-order kinetic equations.

$$v = \frac{Q_e}{T} \quad (2)$$

where, v is the adsorption rate (mg×g^{-1}×min^{-1}), Q_e is the equilibrium adsorption capacity (mg/g) and T is the time (min).

2.4. Desorption experiments

Before the desorption test can be carried out, the preparation of desorption samples is required. 40 g of halloysite-10 Å were placed in a beaker, and 1000 mL of a pH=5.25 mixed RE solution including Nd^{3+}, Eu^{3+}, and Lu^{3+} was added, along with the concentration of 0.5 mmol/L for each RE ion. After 4 hours of mechanical stirring in a beaker, the mixture was permitted to precipitate, and then remove some of the supernatant. The liquid and solid in the solution were separated using centrifugation by transferring it to a 100 mL centrifuge tube. To make sure that the rare earth ions on the clay's surface were adsorbed rather than the unadsorbed portion staying in the solution, deionized water was added after the supernatant was removed. The solid was then broken up and stirred with a glass rod, centrifuged again, and the process was repeated four or five times. The solids were then pulverized into powder as samples for the subsequent desorption experiments under various conditions after being dried in an oven at 105 °C for more than 6 hours. ICP-OES was used to determine the adsorption capacities of Nd^{3+}, Eu^{3+}, and Lu^{3+} in the solid powder.

The desorption process established a halloysite-10 Å/$(NH_4)_2SO_4$ ratio of 1:50, and for the desorption experiment, 0.3 g of the previously adsorbed halloysite-10 Å was taken and 15 mL of the desorption solution $(NH_4)_2SO_4$ was added. Shaking, centrifugation, and filtration, and the concentrations of Nd^{3+}, Eu^{3+}, and Lu^{3+} in the filtrate were assessed using an ICP-OES. Equation (3) was used to determine the desorption efficiency (amount):

$$\xi(\%) = \frac{CV}{MQ_e} \times 100 = \frac{D_m}{Q_e} \times 100 \quad (3)$$

where ξ (%) denotes the efficiency of desorption, C denotes the concentration of rare earth in the desorbed solution (mg/L), V denotes the volume of the desorbed solution (L), M and Qe denote the mass (g) and adsorption capacity (mg/g) of halloysite-10 Å, respectively, Dm denotes desorption amount. In addition, the desorption rate can be calculated by replacing the equilibrium adsorption capacity (Q_e) in Equation (2) by the desorption amount (D_m).

The desorption process was examined at pH values of 2.5, 3, 4, 5, and 6 as well as concentrations of 0, 0.015, 0.0378, 0.0757, 0.1134, and 0.1514 mol/L and contact times of 1, 3, 5, 10, 20, 30, 60, 120, 180, and 240 minutes, respectively, in accordance with the desorption experiment's steps. The desorption test procedure is shown in Fig. 1. Finally, the ideal leaching circumstances were established.

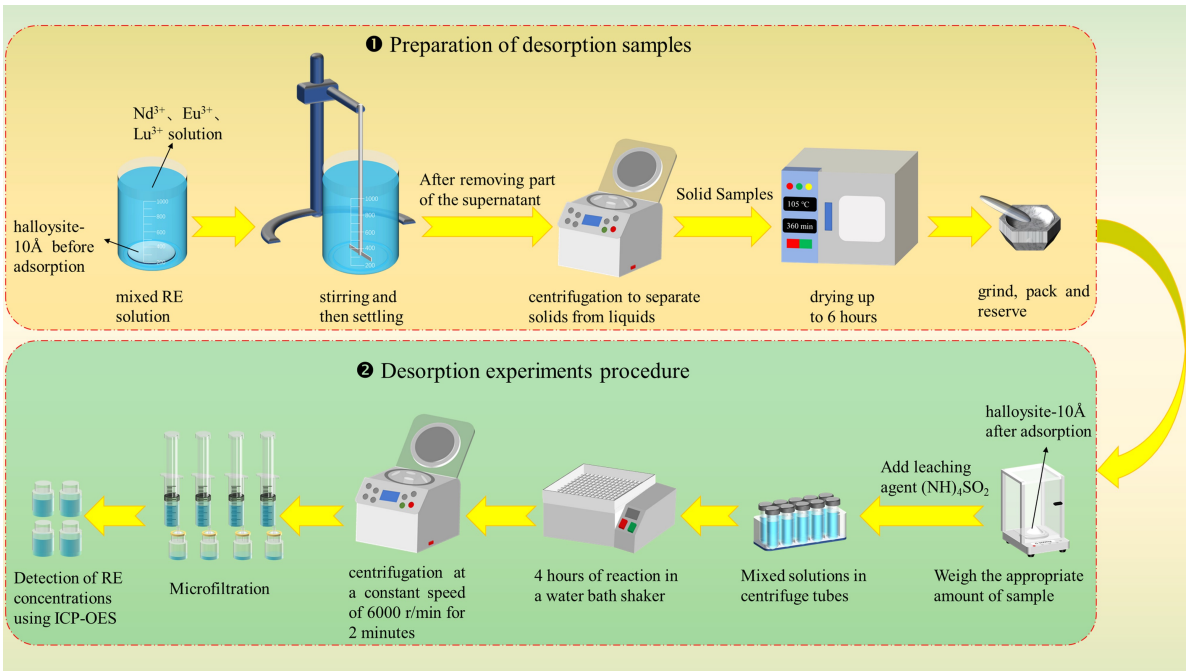

Fig. 1 Diagrammatic schematic for the desorption experiment

3. Results and discussion

3.1. Characterization of halloysite

3.1.1. Analyses using XRD and SEM-EDS

The results of the X-ray diffractometer (XRD) analyses are shown in Fig. 2, which depicts the distinctive diffraction peaks of halloysite-10 Å at 8.836° and 20.352° (2\theta) and the corresponding crystal face spacings of 10.00 and 4.36 for the (001) and (100) faces of halloysite-10 Å, respectively. This indicates that the purity of the chosen halloysite-10 Å is reliable.

SEM was used to describe the morphology of halloysite-10 Å, and an EDS was used to detect the distribution of REEs that had been adsorbing to the surface. The results are displayed in Fig. 3. From the SEM images, it can be observed that the halloysite-10 Å in this study has a flaky structure similar to that of kaolinite (Borst et al., 2020; Gao et al., 2018; Zhou et al., 2022). Additionally, the particle size is relatively fine; it is essentially smaller than 5 μm even after agglomeration has occurred. EDS analysis results reveal that Nd, Eu, and Lu elements are plastered on the clay surface, proving that the REEs have been adsorbed to the surface of halloysite-10 Å.

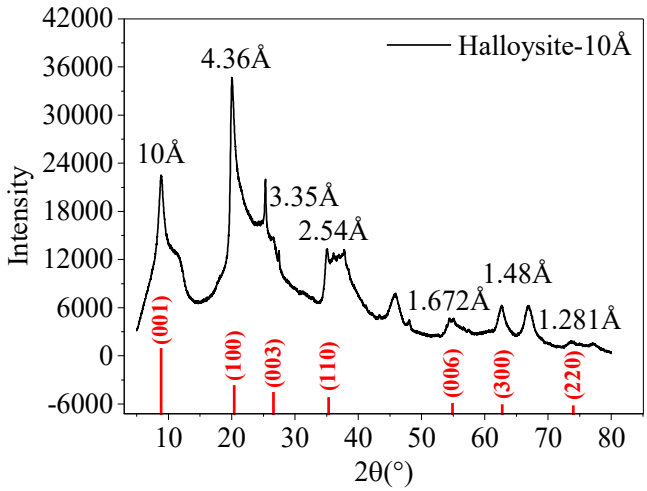

Fig. 2. XRD pattern of halloysite-10 Å

3.1.2. Zeta potential

Zeta potential can be used to reflect the charge of the mineral surface. A higher absolute value of the surface potential indicates a stronger ability to bind "counter-ions" and a greater capacity of "counter-ion" adsorption (Wen et al., 2022). Therefore, the surface charge of halloysite-10 Å is crucial for the adsorption of Nd^{3+}, Eu^{3+}, and Lu^{3+} ions. Before and after the adsorption of halloysite-10 Å, the connection between zeta potential and pH is depicted in Fig. 4. The findings indicate that there is no zero-charge point when the pH ranges between 2.5 and 6. The surface of halloysite-10 Å is negatively charged. For the adsorption of RE ions, the negative surface charge acted as a powerful driving force. Zeta potential considerably decreased with an increase in pH when pH > 3. The surface potential of halloysite-10 Å gradually decreases as pH increases, and to achieve the surface charge balance, many RE ions are adsorbed onto the clay surface. The negatively charged surface aids the mineral particles in adsorbing positively charged ions. Following adsorption, Nd^{3+}, Eu^{3+}, and Lu^{3+} neutralized the majority of the negative charges in the vicinity of the clay, increasing the zeta potential.

3.1.3. Buffering performance

Fig. 5(a) displays the findings of the buffering performance of halloysite-10 Å. Due to the amphoteric hydroxyl group on the surface of halloysite-10 Å, the equilibrium pH is almost constant at 6.5 when the starting pH is in the range of 5 to 10. This shows that halloysite-10 Å has a certain buffering capacity as the protonation reaction happens at low pH to increase the solution pH and the deprotonation reaction occurs at high pH to reduce the solution pH. Fig. 5(b) illustrates how time affects the protonation and deprotonation processes of halloysite-10 Å. The pH values at 1 min are 5.04 (initial pH=3) and 8.94

(initial pH = 11), and the process essentially approaches equilibrium within 20 minutes, which suggests that the protonation and deprotonation reaction proceeds swiftly. The equilibrium pH was 5.65 and 8.5 when the initial pH was 3 and 11, respectively, indicating that there is a limit to the buffering capacity of halloysite-10 Å.

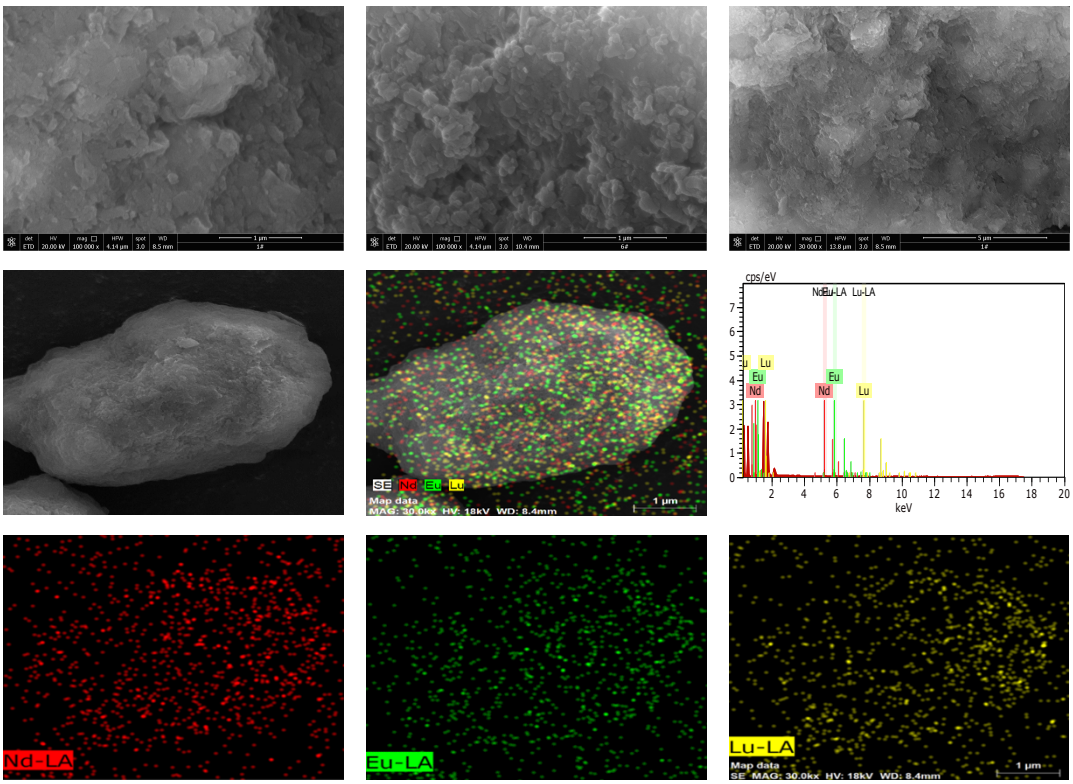

Fig. 3. SEM-EDS images for halloysite-10 Å

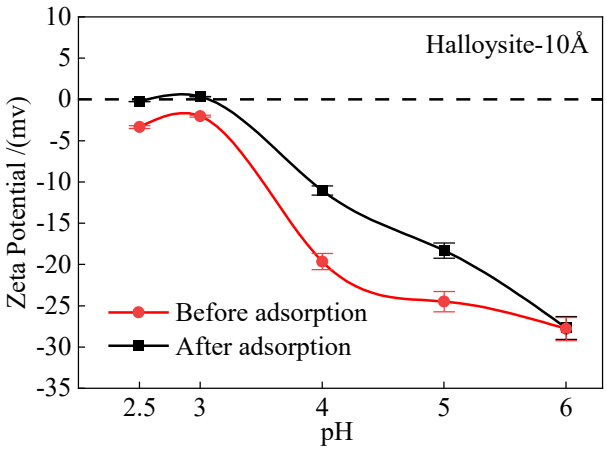

Fig. 4. Zeta potential halloysite-10 Å as a function of pH

3.2. Adsorption characteristics of Nd^{3+}, Eu^{3+}, and Lu^{3+} by halloysite-10 Å

3.2.1. Effect of concentration on the adsorption process of Nd^{3+}, Eu^{3+}, and Lu^{3+}

Fig. 6 illustrates the correlation between the capacity of adsorption and various concentrations of Nd^{3+}, Eu^{3+}, and Lu^{3+} solutions. The findings demonstrate that halloysite-10 Å exhibits preferential adsorption of the heavy RE ion (Lu^{3+}), a trend that becomes more pronounced with increasing RE concentration, and that the adsorption of the three RE ions by halloysite-10 Å increases gradually with increasing RE concentration. The reason for the high adsorption capacity at high concentrations is that the concentration difference between the adsorbent and the high-concentration solution acts as a mass transfer driving force, allowing the RE ions to overcome the resistance to movement in the solid-liquid

phase (Guan et al., 2022). In addition, at high concentrations of RE solution, the active adsorption sites on the surface of halloysite-10 Å are surrounded by more RE ions, which can considerably raise the likelihood of effective collisions (Zhou, F et al., 2021). Due to this increased likelihood of reaching adsorbable sites on the clay surface when RE ions are present in high concentration, larger adsorption capacities are achieved. As for Lu^{3+}, its lower ionic radius may be responsible for the large capacity of adsorption that it exhibits.

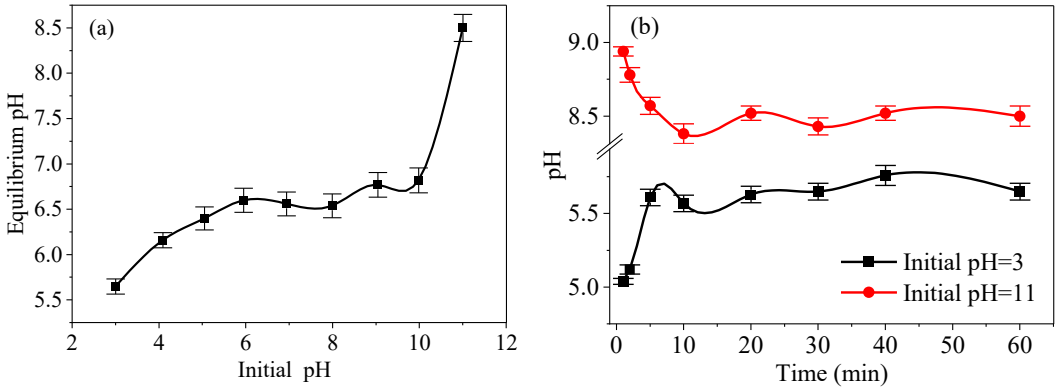

Fig. 5. Buffering performance of halloysite-10 Å (a) and the effect of time on protonation and deprotonation reactions (b)

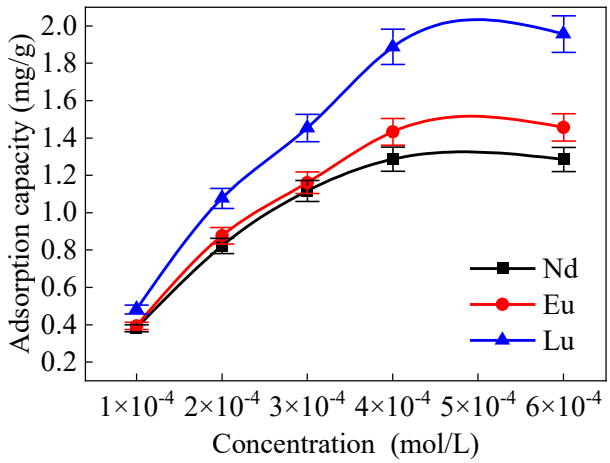

Fig. 6. Effect of concentration on Nd^{3+}, Eu^{3+}, and Lu^{3+} adsorption on halloysite-10 Å

For analyzing the regulation mechanisms of adsorption processes, researchers often turn to Langmuir and Freundlich isotherms. These particular equations are listed below:

- Langmuir equation:

$$Q_e = \frac{K_L Q_m C_e}{1+K_L C_e} \tag{4}$$

- Freundlich equation:

$$Q_e = K_F \cdot C_e^{\frac{1}{n}} \tag{5}$$

where Q_e is the appropriate adsorption amount (mg/g), C_e is the solution concentration at adsorption equilibrium (mg/L), Qm is the maximum adsorption capacity (mg/g), K_L, K_F, and n are parameters.

In contrast to the Freundlich isotherm equation, which assumes a non-homogeneous multimolecular layer adsorption surface, the Langmuir isotherm equation assumes that the adsorption surface is homogeneous and monomolecular layer adsorption (Wang et al., 2019). The fitting curves for the Langmuir and Freundlich models for the adsorption of Nd^{3+}, Eu^{3+}, and Lu^{3+} by halloysite-10 Å are shown in Fig. 7. Table 1 is a list of the pertinent isothermal adsorption parameters. According to the results of the fitting, the correlation parameter (R2) for the Langmuir isotherm fitting for all three RE ions is close to 0.95, which is significantly higher than that of the Freundlich isothermal adsorption

model, which suggests that the binding sites on the surface of halloysite-10 Å are uniformly distributed and that Nd^{3+}, Eu^{3+}, and Lu^{3+} adsorb to their surfaces as mono-molecular layer adsorption. The adsorption of Nd^{3+}, Eu^{3+}, and Lu^{3+} on halloysite-10 Å is thought to be regulated by chemical adsorption because it is commonly accepted that physical adsorption controls multimolecular layer adsorption whereas chemical adsorption forms monolayer adsorption.

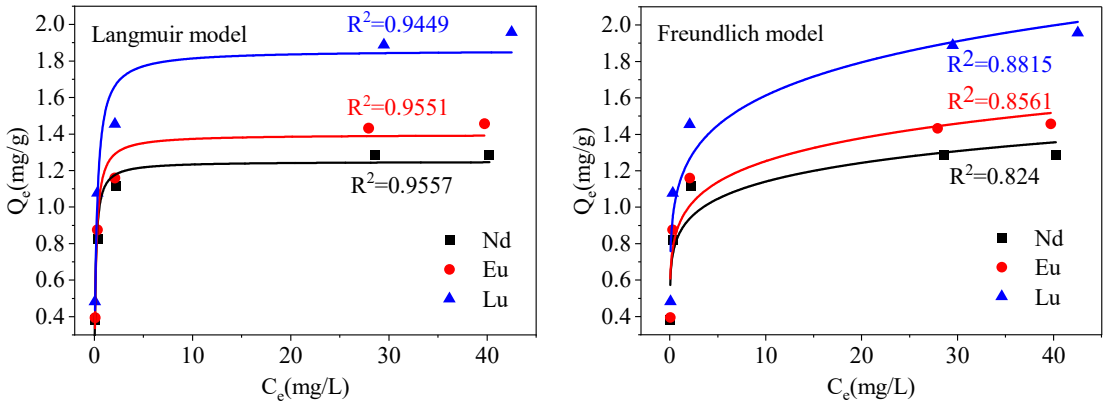

Fig. 7. Langmuir and Freundlich isothermal adsorption fitting results for Nd^{3+}, Eu^{3+}, and Lu^{3+} on halloysite-10 Å

Table 1. Langmuir and Freundlich isothermal adsorption parameters of Nd^{3+}, Eu^{3+}, and Lu^{3+} on halloysite -10 Å

Element	Langmuir		Freundlich		
	K_L $(L \cdot g^{-1})$	R^2	K_F $(m\,g \cdot g^{-1}) \cdot (mg \cdot L^{-1})^{-1/n}$	n	R^2
Nd	7.6478	0.9557	0.8558	8.0192	0.8240
Eu	5.7711	0.9551	0.9099	7.2023	0.8561
Lu	4.0708	0.9449	1.1305	6.4796	0.8815

3.2.2. Effect of time on the adsorption process of Nd^{3+}, Eu^{3+}, and Lu^{3+}

Fig. 8(a) shows the relationship between the capacity of adsorption and the contact time. In the first 30 minutes, the amounts of Nd^{3+}, Eu^{3+}, and Lu^{3+} that were adsorbed on halloysite-10 Å grew quickly with time. After that, the levels climbed gradually until they essentially leveled off after 60 minutes. In Fig. 8(b), the findings of the Nd^{3+}, Eu^{3+}, and Lu^{3+} adsorption rates with time are displayed. The adsorption rates of Nd^{3+}, Eu^{3+}, and Lu^{3+} all displayed the same downward trend over time; the adsorption rate dropped sharply from 0 to 30 minutes. then changed very slowly from 30 to 240 minutes. Additionally, the Nd^{3+}, Eu^{3+}, and Lu^{3+} adsorption levels reached more than 95% after 30 minutes, showing that the adsorption process was primarily carried out during the first 30 minutes. RE ions can be absorbed quickly since there are a lot of available vacancies on halloysite-10 Å for them to fill within 0~30 minutes. Adsorption equilibrium is reached when RE ions have fully occupied the majority of the adsorbable sites on the surface of halloysite-10 Å throughout the adsorption process (Guan et al., 2022). In the meantime, it is discovered that the adsorption capacity rises in the following order: $Nd^{3+} < Eu^{3+} < Lu^{3+}$, which corresponds to the progression from light to heavy REEs. It is possible to connect the "lanthanide contraction phenomenon" to the preferential adsorption of heavy RE ions by clay materials (Coppin et al., 2002). Additionally, when the outer surface's adsorption sites are full, heavy RE with lower ionic radii can be adsorbed on the inner surface by diffusing into the adsorbent's pores and occupying more adsorption sites, resulting in higher adsorption capacity than light RE.

In order to further study the control mechanism of the adsorption process, the kinetic behavior of rare earth ions on halloysite-10 Å was examined by using pseudo-first-order and pseudo-second-order kinetic equations. These particular equations are listed below:

- The pseudo-first-order model:

$$ln(Q_e - Q_t) = lnQ_e - K_1 t \tag{6}$$

- The pseudo-second-order model:

$$\frac{t}{Q_t} = \frac{1}{Q_e} t + \frac{1}{K_2 Q_e^2} \tag{7}$$

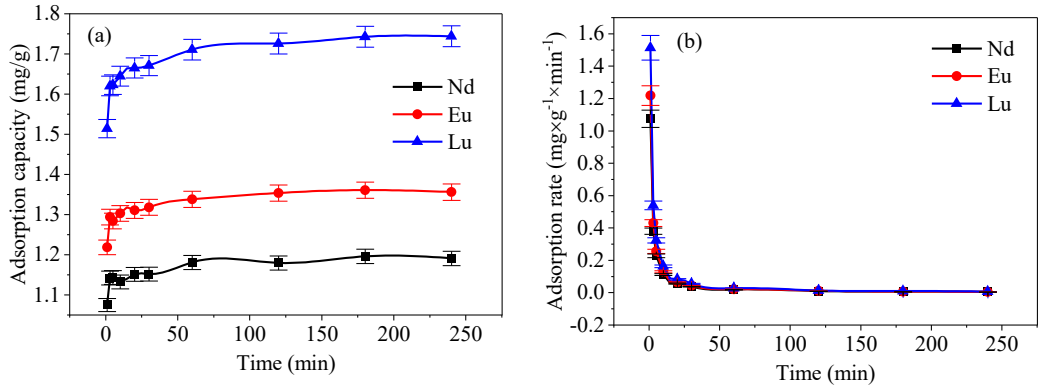

Fig. 8. Effect of time on the adsorption of Nd^{3+}, Eu^{3+}, and Lu^{3+} on the surface of halloysite-10 Å (a) and the curve of the adsorption rate of Nd^{3+}, Eu^{3+}, and Lu^{3+} as a function of time (b)

where Q_e and Q_t are the adsorption capacities at equilibrium and time t (mg/g), respectively, and K_1 and K_2 are the corresponding kinetic parameters.

The fitted curves for the adsorption kinetics of Nd^{3+}, Eu^{3+}, and Lu^{3+} on halloysite-10 Å are shown in Fig. 9. Table 2 displays the corresponding pseudo-first-order and pseudo-second-order kinetic parameters. The pseudo-second-order kinetic model's correlation coefficients (R2) for the adsorption kinetics of the three RE ions reached 0.999, which is higher than that of the pseudo-first-order kinetic model. The experimental values of 1.197, 1.356, and 1.744 were extremely close to the Qe values derived by fitting, which were 1.198, 1.359, and 1.747, respectively. The results show that the pseudo-second-order kinetic model is able to more accurately reflect the adsorption kinetic behavior of Nd^{3+}, Eu^{3+}, and Lu^{3+} on the halloysite-10 Å surface, suggesting that both the concentration of the rare earth ions and the number of active sites on the clay affect the rate of adsorption (Zhou et al., 2018), and also this implies that the adsorption processes of Nd^{3+}, Eu^{3+}, and Lu^{3+} are predominantly chemisorptive (Zhou et al., 2021). The results of this study are consistent with the conclusion of isothermal adsorption fitting.

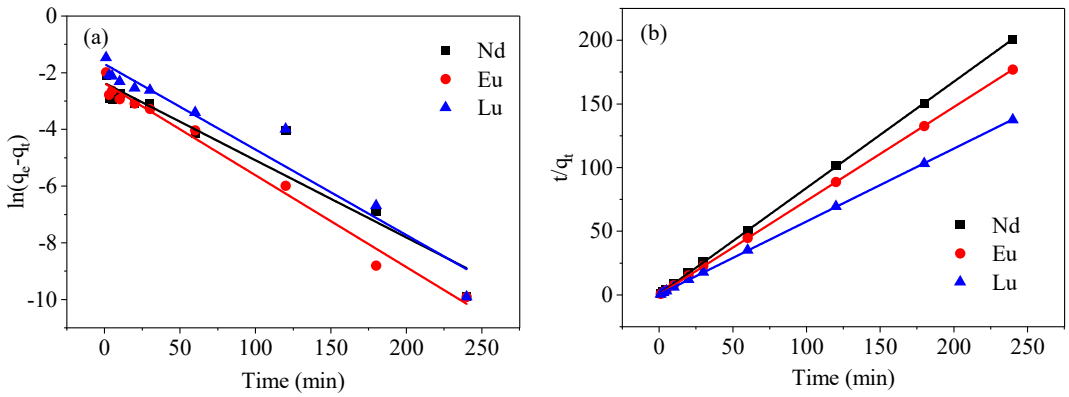

Fig. 9. Pseudo-first-order (a) and pseudo-second-order (b) kinetic modelling of Nd^{3+}, Eu^{3+}, and Lu^{3+} on halloysite-10 Å

Table 2. Pseudo-first-order and pseudo-second-order kinetic parameters of Nd^{3+}, Eu^{3+}, and Lu^{3+} on halloysite-10 Å

Element	Pseudo-first-order			Pseudo-second-order		
	Q_e (mg/g)	K_1 (min^{-1})	R^2	Q_e (mg/g)	K_2 ($g \cdot mg^{-1} \cdot min^{-1}$)	R^2
Nd	0.094	0.027	0.909	1.198	1.354	0.999
Eu	0.093	0.032	0.985	1.359	1.563	0.999
Lu	0.184	0.030	0.941	1.747	0.789	0.999

3.2.3. Effect of pH on the adsorption process of Nd^{3+}, Eu^{3+}, and Lu^{3+}

The adsorption of Nd^{3+}, Eu^{3+}, and Lu^{3+} on halloysite-10 Å as a function of pH is depicted in Fig. 10. According to the figure, the amounts of Nd^{3+}, Eu^{3+}, and Lu^{3+} that were adsorbed on halloysite-10 Å increased gradually as the pH value increased, and these amounts were 1.14 mg/g, 1.35 mg/g, and 1.56

mg/g, respectively, at the pH value of 4.76. The adsorption capacities remained unchanged as pH was raised to 5.76, indicating that the halloysite-10 Å adsorption sites were saturated. Nd^{3+}, Eu^{3+}, and Lu^{3+} adsorption capacities at pH=2.01 were 0.357 mg/g, 0.34 mg/g, and 0.34 mg/g, respectively, which were significantly lower than those at pH=4.76 and 5.76. The reason for this is due to two factors: on the one hand, the presence of many high concentrations of H^+ in the low pH solution will compete with the RE ions for adsorption, resulting in fewer RE ions being adsorbed onto the surface of the clay minerals; on the other hand, with an increase in pH, the deprotonation reaction occurs, causing the clay surface to expose more adsorbable sites and adsorb more RE ions in the form of inner layer adsorption (Yang et al., 2019). As a result, adsorption capacity at high pH is substantially greater than at low pH.

In the initial pH range of 2.01 to 5.76, the equilibrium pH before and after the adsorption of Nd^{3+}, Eu^{3+}, and Lu^{3+} on halloysite-10 Å were examined. The findings are displayed in Fig. 10. The range of the equilibrium pH following adsorption, which varied from 4.96 to 5.86 and was different from the initial pH, further demonstrated the buffering performance of the halloysite-10 Å. Both the equilibrium pH and the increased trend of the adsorption capacity stabilized at pH=4.76, which also showed that the equilibrium pH rather than the starting pH was what affected the adsorption capacity. Additionally, the equilibrium pH was a little lower than the buffer pH, indicating that some H^+ escaped from the clay surface during adsorption (Qiu et al., 2022b).

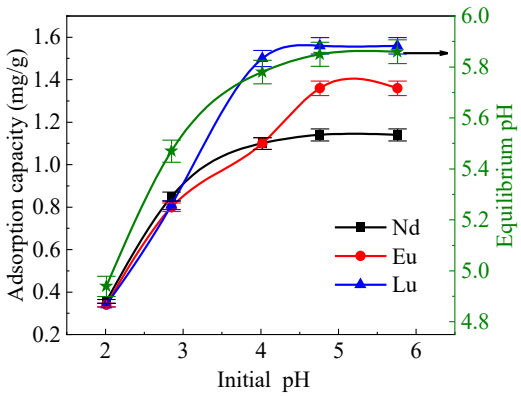

Fig. 10. Effect of pH on Nd^{3+}, Eu^{3+}, and Lu^{3+} adsorption on halloysite-10 Å

3.2.4. Investigations of differential adsorption between Nd^{3+}, Eu^{3+}, and Lu^{3+}

The adsorption capacity and ionic radius presented an intriguing correlation in the adsorption tests mentioned above, and the adsorption capacity was inversely proportional to the ionic radius. This relationship was satisfied as Nd^{3+} (0.99 Å) < Eu^{3+} (0.95 Å) < Lu^{3+} (0.85 Å) for the three RE ions, ionic radius data from literature (Moldoveanu and Papangelakis, 2012). It can be assumed that the selective adsorption of REE by clay minerals is due to the ionic radius, the lower the ionic radius exhibit stronger the contact with the clay surface and the larger the adsorption capacity (Moldoveanu and Papangelakis, 2012). In accordance with previous studies: the adsorption of halloysite-7 Å (Zhejiang, China) in the K^+ system diminishes as the atomic number of REE increases, but kaolinite exhibits the opposite trend (Gao et al., 2018). Under 0.5 mol/L NaNO3 ionic strength, halloysite-7 Å (Linfen, Jiangxi, China) showed an increase in its logKd value (Kd is the adsorption coefficient, mL/g) as atomic number increased (Yang et al., 2019). By using oscillatory adsorption, (Qiu et al., 2022b) discovered that halloysite-7 Å (Yunnan, China) adsorbed Nd, Eu, and Lu in the following order: Lu > Nd > Eu. The order of kaolinite's adsorption capacities on La, Nd, and Y is La > Nd > Y, as demonstrated by (Xiao et al., 2016a). The above studies show that the adsorption variability between different RE ions and the radius of the RE ions is not a simple linear relationship, but is related to the type of clay minerals, the source, and the experiment conditions (including ionic strength, ionic species, reaction mode, etc.), and so on.

3.3. Desorption characteristics of Nd^{3+}, Eu^{3+}, and Lu^{3+} by halloysite-10 Å

3.3.1. Effect of pH on desorption efficiency

The impact of various adsorption pH on the desorption efficiency was examined to reveal the adsorption mechanism at various pH levels. The outcomes are displayed in Fig. 11(a). The desorption

efficiency gradually decreased with the increase of adsorption pH, and the desorption efficiencies of Nd^{3+}, Eu^{3+}, and Lu^{3+} were more than 99% at the adsorption pH=2.01, indicating that the adsorbed RE ions could be desorbed basically in full at this time; when the adsorption pH was higher than 2.01, the desorption efficiencies of Nd^{3+}, Eu^{3+}, and Lu^{3+} were significantly reduced with the increase of the adsorption pH and gradually leveled off after the adsorption at pH=4.76. Utilizing density functional theory calculations, researchers (Yan et al., 2022; Qiu, T.S et al., 2021., Qiu, S et al.,2021) discovered that hydrated rare earth ions can, via hydrogen bonding and ligand bonding effects, produce an outer layer adsorption and a more stable inner layer adsorption on the kaolinite surface, respectively. Parallel to this, at low pH, the protonation reaction on the surface of halloysite-10 Å leads to the adsorption of rare earth ions on the clay surface in the form of outer layer adsorption, mostly via electrostatic attraction to form hydrogen bonds, which are easily removed by NH^{+4}; as the adsorption pH increases, the deprotonation reaction occurs so that the RE ions are adsorbed on the clay surface in a more stable inner layer adsorption form (Qiu, T.S et al., 2021; Qiu et al., 2022a). The intimate adsorption between the clay surface and rare earth ions in the inner layer of the adsorption results in a pH of 4.76 ammonium sulfate that is difficult to completely desorb, lowering the rate of desorption and necessitating the use of a solution with higher acidity to leach.

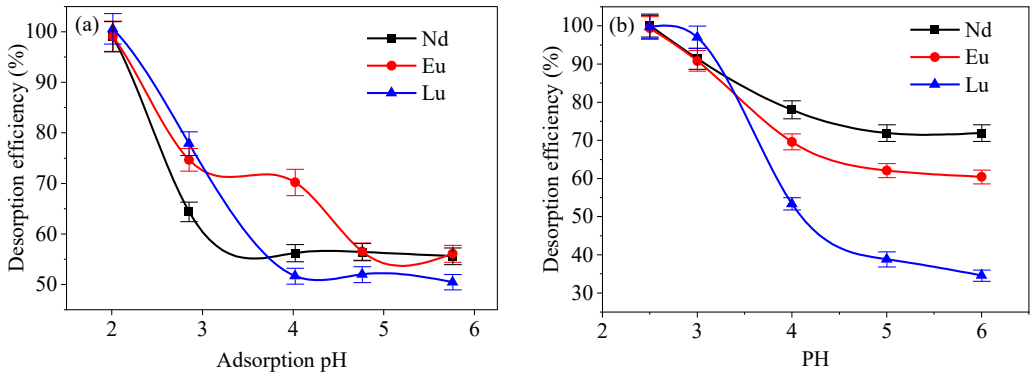

Fig. 11. Effect of adsorption pH (a) and desorption pH (b) on the desorption of Nd^{3+}, Eu^{3+}, and Lu^{3+} from halloysite-10 Å (pH = 4.76 (a), reaction time = 240 min, $(NH_4)_2SO_4$ concentration = 0.1134 mol/L)

The link between the pH of the desorption solution and the desorption efficiencies of Nd^{3+}, Eu^{3+}, and Lu^{3+} is depicted in Fig. 11(b). All three RE ion desorption efficiencies were near 100% at pH=2.5, and it can be seen that their desorption efficiencies all dropped as pH increased. The desorption efficiencies of Nd^{3+}, Eu^{3+}, and Lu^{3+}, however, showed a clear decline with the increase in pH when the pH range was 4~6, particularly Lu3+ ion, whose desorption efficiency dropped from 99.74% (pH=2.5) to 34.58% (pH=6.0), a decrease of about 65%, and the corresponding desorption efficiencies of Nd^{3+} and Eu^{3+}, which fell by 28% and 39%, respectively. The two explanations that follow can both be used to explain this phenomenon: On the one hand, Nd^{3+}, Eu^{3+}, and Lu^{3+} can be adsorbed on the surface of halloysite-10 Å in the form of inner layer adsorption, as was previously mentioned. However, the partial (or complete) dehydration of hydrated RE ions during the inner layer adsorption process causes the RE ions to form stable adsorption through ligand bonding by binding them directly to the Al-O or Si-O on the surface or edges of the clay (Borst et al., 2020), and the low acidity ammonium sulfate solutions are difficult to desorb them down. However, they can be transformed into more readily desorbed outer layer adsorption by electrostatic attraction in low pH environments (Qiu et al., 2022b). Therefore, the desorption efficiency considerably lowers as pH increases. On the other hand, Lu^{3+} presents a lower desorption efficiency, which may be attributed to the hydrolysis of RE ions. The RE ions adsorbed on the surface of the clay undergo hydrolysis to form stable chemisorbed species $clay \equiv REE(OH)_3$. It has been demonstrated (Moldoveanu and Papangelakis, 2012; Moldoveanu and Papangelakis, 2013) that hydrolysis of rare earth ions also occurs at pH=5, and the hydrolysis tendency increases with the contraction of the atomic number and atomic radius. As a result, in contrast to Nd^{3+}, Eu^{3+}, and Lu^{3+} displayed a very low desorption efficiency at pH=5 and 6. Nd^{3+}, Eu^{3+}, and Lu^{3+} have the best desorption effects at a pH of 2.5, and the hydrolysis of RE ions can be completely disregarded at this pH value. Additionally, higher acidity can greatly avoid the reduction in rare earth leaching efficiency and the

waste of leaching agents due to the phenomenon of rare earth ions re-adsorption. Thus, it is best to select an ammonium sulfate solution with a pH of 2.5.

3.3.2. Effect of concentration on desorption efficiency

The desorption of Nd^{3+}, Eu^{3+}, and Lu^{3+} from the surface of halloysite-10 Å is depicted in Fig. 12(a) as a function of various ammonium sulfate concentrations. The desorption efficiencies of Nd^{3+}, Eu^{3+}, and Lu^{3+} have been close to or even more than 60% in pure acid solutions, demonstrating that H^+ participates in the ion exchange process and that the high acidity is favorable for the desorption of RE ions. The desorption efficiency dramatically increased after employing an ammonium sulfate solution. The desorption efficiency gradually increased with the amount of $(NH_4)_2SO_4$ added, reaching a plateau and then essentially leveling out at 5 g/L. The findings indicated that the desorption of REEs by acid can be greatly improved by the presence of ammonium sulfate (Xu et al., 2018). The ability of the leaching agent to penetrate deeply into the interior of clay particles was improved with an increase in ammonium sulfate concentration, and it became simpler to access the RE ion adsorption sites and exchange them. At a concentration of 15 g/L ammonium sulfate, the desorption efficiencies of Nd^{3+}, Eu^{3+}, and Lu^{3+} were all nearly 99%. It was determined that 15 g/L of ammonium sulfate was the ideal concentration for the desorption of RE ions from the surface of halloysite-10 Å.

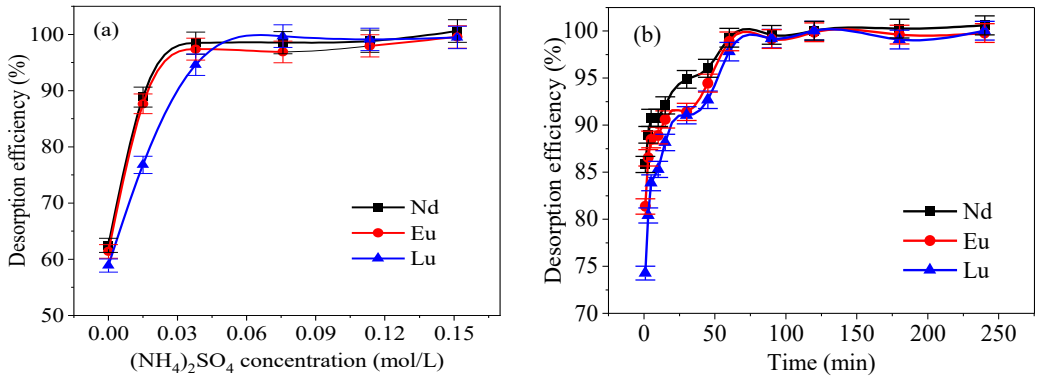

Fig. 12. Effect of $(NH_4)_2SO_4$ concentration (a) (reaction time = 240 min, pH =4.76) and time (b) (pH =2.5, $(NH_4)_2SO_4$ concentration = 0.1134 mol/L) on the desorption of Nd^{3+}, Eu^{3+}, and Lu^{3+} from halloysite-10 Å

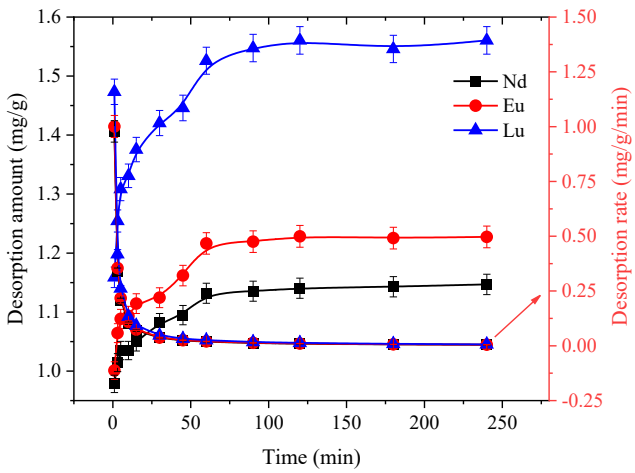

Fig. 13. Desorption amount and desorption rate versus time curves for halloysite-10 Å (pH =2.5, $(NH_4)_2SO_4$ concentration = 0.1134 mol/L)

3.3.3. Effect of time on desorption efficiency

Under the conditions of $(NH_4)_2SO_4$ concentration of 15 g/L and pH=2.5, the influence of varied time on the desorption efficiency was examined. The results are shown in Fig. 12(b) and Fig. 13, where the desorption efficiency increased and subsequently leveled off with the increase of contact time. The desorption rates of the three RE ions were not significantly different, the desorption rates decreased

linearly from 0 to 15 min, the desorption rates were very fast, and the desorption rate was more than 90% in 15 min (except for Lu^{3+}, 88%), which indicated that the leaching process mainly occurred in the first 15 min. In the stage of 30-60 min, there was a small decrease in the desorption rates, and from 60 to 240 min, desorption rate curves flatten out. The desorption rates (amounts) did not change with time, and the desorption equilibrium was reached at this time. The desorption amounts of Lu^{3+} were the highest, followed by Eu^{3+} and Lu^{3+}, which was consistent with the order of adsorption capacities (Lu^{3+} > Eu^{3+} > Nd^{3+}), and the higher adsorption capacities led to the higher desorption amounts. The equilibrium desorption efficiencies of Nd^{3+}, Eu^{3+}, and Lu^{3+} were all more than 99%, which indicated that the adsorption of RE ions on the surface of halloysite-10 Å was basically completely desorbed. This is because, in the right conditions—high acidity and appropriate concentration of ammonium sulfate—both the inner and outer adsorbed RE ions can be entirely desorbed. When seen in conjunction with Figs. 10(b) and 11(a), it is evident that pH has the biggest impact on the RE ions desorption process.

3.3.4. Examination of halloysite's desorption characteristics

In contrast to tubular halloysite-7 Å (Qiu et al., 2022b), the desorption efficiency of halloysite-10 Å was significantly impacted by the pH of the adsorption and desorption solution. This suggests that the platy structure of halloysite-10 Å has a greater influence on its desorption behavior, leading to a significant difference between halloysite-10 Å and halloysite-7 Å. Furthermore, it has been observed that the Al-OH group of halloysite exhibits a greater affinity for RE ions compared to the Si-O-Si group (Tertre et al., 2006). On aluminum-oxygen octahedra, RE ions can form both inner and outer layer adsorption through ligand bonding and hydrogen bonding, while on silica-oxygen tetrahedra, they can only form a weak outer layer adsorption (Yan et al., 2022). The silica-oxygen tetrahedra in tubular halloysite are located outside, while the aluminum-oxygen octahedra are convoluted in the inner space. As a result, RE ions find it difficult to pass through the narrow layer spacing of halloysite-7 Å. Ultimately, most RE ions form an outer layer adsorption within the silica-oxygen tetrahedra through electrostatic interactions, RE ions adsorbed in this form are more readily desorbed, and therefore, the desorption efficiency varies less with pH (Qiu et al., 2022b). The platy structure of halloysite, which consists of silica-oxy tetrahedron and aluminum-oxy octahedron, makes it easier for RE ions to form stable inner layer adsorption on the aluminum-oxy octahedron through ligand bonding, which is much more difficult to desorb than the outer layer of adsorption on silica-oxy tetrahedron. The efficiency of desorption is highly dependent on pH, meaning that perfect leaching is only possible at low pH levels. Furthermore, RE ions can travel through halloysite-10 Å more readily because of its high layer spacing, and some of these REs may be present inside the mineral as interlayer adsorbed states (Zhou, J M et al., 2021).

The chemical compositions of halloysite and kaolinite are remarkably similar. Halloysite, also known as polyhydric kaolinite, is difficult to recognize them, while the crystal structures are quite different (kaolinite is mostly platy, while halloysite is tubular). The halloysite-10 Å in this study has a platy structure, which exhibits less variations between halloysite and kaolinite, the degree of hydration is currently the primary distinction between the two. Compared to kaolinite, which has an interlayer spacing of 0.72 nm, halloysite-10 Å has a greater interlayer spacing of 1 nm due to the presence of interlayer water molecules. The desorption behavior of halloysite-10 Å is more akin to that of kaolinite (Qiu et al., 2022a; Qiu et al., 2022c) due to its extremely comparable chemical composition and crystal structure.

In the Huangshe rare earth mining area of Renju town, Meizhou city, Guangdong Province, China, Yang et al. (2019) discovered that the halloysite content rose with depth (12.6-23.4 m), although kaolinite did exhibit the opposite tendency. Furthermore, the clay minerals in the lower portion of the weathered crust have a higher cation exchange capacity (CEC) because they are often less crystalline, have small grain sizes, and have a high specific surface area. Even though montmorillonite and illite have significant CEC, they are mostly found in the semi-weathered layer, which is far from the topsoil layer and has fewer ionic-phase rare earths, while kaolinite and halloysite are mainly located in the fully weathered layer (Liang et al., 2022). Compared to halloysite-7 Å, halloysite-10 Å has a greater CEC. The enrichment of RE ions is facilitated by higher concentrations of halloysite-10 Å in weathered crustal lacustrine rare earth deposits (Ram et al., 2019; Zhou, J M et al., 2021), and therefore halloysite-10 Å deserves more attention. The study's findings can offer some potential recommendations for RE

leaching technology: To achieve high efficiency and low-cost leaching of REs, the optimal leaching scheme can be formulated independently based on the distribution status of different clay minerals and the variety of desorption behaviors in the ionic rare earth deposits. If the predominant clay in ionic rare earth ores is halloysite-10 Å, as is the case with halloysite in the Xishuangbanna district of Yunnan (Li et al., 2016), then the leachate pH must be less than 3 and the leaching duration must be extended during the leaching process. However, our research is still lacking: perhaps it is necessary to further construct the adsorption model of halloysite-10 Å and identify the most stable hydration configurations of the three RE ions and so on through density-functional theory analysis. This will allow us to ascertain the adsorption stability of REs by calculating adsorption energies, bond lengths, and other relevant parameters, as well as to uncover the differential law of the adsorption process of various RE ions from a microscopic perspective.

4. Conclusions

The adsorption capacities of light (Nd^{3+}), medium (Eu^{3+}), and heavy (Lu^{3+}) rare earth ions by halloysite-10 Å increased with the increase of adsorption pH, and basically remained stable at pH higher than 4, and exhibited some selectivity for heavy rare earths. The adsorption process of Nd^{3+}, Eu^{3+}, and Lu^{3+} by halloysite-10 Å is consistent with the Langmuir isothermal adsorption model and pseudo-second-order model. The results indicate that the adsorption process belongs to monomolecular layer adsorption and is controlled by chemisorption. Protonation and deprotonation of amphiphilic hydroxyl groups on the surface of halloysite-10 Å is a significant factor affecting the adsorption process. At low pH levels, protonation reaction on the surface of halloysite-10 Å occurs, and RE ions are adsorbed on the clay surface in the form of outer layer adsorption primarily through electrostatic attraction; however, at higher pH levels, deprotonation reaction occurs on the surface of halloysite-10 Å, which causes the negative charge on the surface of the clay to gradually increase, leading to the formation of a more stable inner layer of adsorption of the RE ions on the surface of the clay.

The desorption efficiency of halloysite-10 Å in the pH range studied in this paper (pH=2.5~6) decreases with increasing pH, and the desorption efficiencies of Nd^{3+}, Eu^{3+}, and Lu^{3+} are all close to 100% when pH=2.5, but they decrease to 71.93%, 60.44%, and 34.58%, respectively, when pH=6. Lower desorption efficiency of Lu^{3+}: On the one hand, this is due to more Lu^{3+} adsorbs as inner layer adsorption, which is more challenging to desorb in high pH solutions; on the other hand, under high pH conditions, Lu^{3+} undergoes hydrolysis and subsequently forms stable chemisorbed species, which results in the desorption efficiency of Lu^{3+} being significantly lower than that of Nd^{3+} and Eu^{3+} at high pH. The desorption kinetics results showed that there was no discernible difference in the desorption rates of light, medium, and heavy rare earth ions and that all desorption rates were extremely rapid, reaching more than 90% at 15 min (with the exception of Lu^{3+}, which was 88%), and the desorption equilibrium was reached at 60 min.

Acknowledgements

The authors gratefully acknowledge the support from the National Natural Science Foundation of China (No. 52274262 and 52004107), Jiangxi Province "Ganpo Juncai" Support Program - Training Program for Academic and Technical Leaders in Major Disciplines (Young Talents) (No. 20232BCJ23005), Jiangxi Outstanding Youth Fund Project (No. 20232ACB214008), Jiangxi Natural Science Foundation (No. 20224BAB204036), General Projects of Key R&D Programs of Jiangxi Province (No. 20212BBG73049), National innovation and entrepreneurship Training Program for college students (No. 202110407032).

References

BORST, A.M., SMITH, M.P., FINCH, A.A., ESTRADE, G., BENAVENT, C.V., NASON, P., MARQUIS, E., HORSBURGH, N.J., GOODENOUGH, K.M., XU, C., KYNICKY, J., GERAKI, K., 2020. *Adsorption of rare earth elements in regolith-hosted clay deposits*. Nature Communications. 11, 4386.

CHEN, X., HE, Q., CHEN, J.F., HUANG, L., TAN, C.M., YIN, Y.Q., JIAO, Y.F., XIAO, Y.F., 2022. *Development of leaching technology and theory of ion-adsorption type rare earth ore*. Journal of the Chinese society of rare earths. 40, 936-947.

CHI, R.A., TIAN, J., *Hydrometallurgy of the Weathered Crust Elution-Deposited Rare Earth Ores*. Beijing: Science Press, 2006.

CHI, R.A., TIAN, J., 2007. *Review of weathered crust rare earth ore*. Journal of the Chinese Rare Earth Society. 6, 641-650.

CHI, R.A., TIAN, J., LUO, X.P., XU, Z.G., HE, Z.Y., 2012. *The basic research on the weathered crust elution-deposited rare earth ores.* Nonferrous Metals Science and Engineering. 3, 1-13.

COPPIN, F., BERGER, G., BAUER, A., CASTER, S., LOUBET, M., 2002. *Sorption of lanthanides on smectite and kaolinite.* Chemical Geology. 182, 57-68.

DUAN, K.B., WANG, D.H., LIU, Q.Y., LI, J., DUAN, X.F., WANG, Y., LI, H., DOU, S.X., 2014. *Feasibility study on REE-bearing phosphate ore directly used for the production of REE phosphate fertilizer in Zhijin, Guizhou*. Resources & Industries. 20, 42-50.

GAO, Y.H., FAN, Z.C., XU, H., WANG, L., 2018. *An experimental study of the characteristics of REE adsorption of kaolinite and halloysite-7 Å*. Acta Petrologica et Mineralogica. 37, 161-168.

GUAN, X.D., LI, P., LIU, W.K., CHANG, Q.Q., HAN, Y.W., ZHANG, J.K., ZHANG, H.L., LI, Q., ZHENG, S.L., 2022. *Adsorption mechanism of yttrium ions onto ion-adsorption type rare earths ore*. Separation and Purification Technology. 299, 121641.

HAN, L.X., YAN, C.J., ZHAO, J., XU, T., 2011. *Study on purification of halloysite nanotubes*. Conservation and Utilization of Mineral Resources. 31, 36-40.

HUANG, L.H., 2006. *Rare earth extraction technology*. Beijing: Metallurgical Industry Press.

JIN, J.Q., ASSEMI, S., ASGAR, H., GADIKOTA, G., TRAN, T., NGUYEN, W., MCLENNAN, J.D., MILLER, J.D., 2021. *Characterization of Natural Consolidated Halloysite Nanotube Structures*. Minerals. 11, 1308.

JOUSSEIN, E., PETIT, S., CHURCHMAN, J., THENG, B., RIGHI, D., DELVAUX, B., 2005. *Halloysite clay minerals – a review.* Clay Minerals. 40, 383-426.

LI, X.F., GUAN, J.F., CHENG, F.F., ZHANG, F., YIN, K., 2016. *Characteristics of halloysite from Xishuangbanna area, Yunnan Province, China.* Acta Mineralogica Sinica. 36, 138-142.

LIANG, X.L., TAN, W., MA, L.Y., ZHU, J.X., HE, H.P., 2022. *Mineral surface reaction constraints on the formation of ion-adsorption rare earth element deposits*. Earth Science Frontiers. 29, 29-41.

LIU, C.L., HUANG, J.H., YAN, H.Z., KONG, F.Q., 2007. *Status and prospect of research on rare earth red pigment for ceramics.* Chinese Rare Earths. 28, 88-91.

MA, Y.H, 2000. *Current status and prospects of rare earth applications in China*. Materials Reports. 14, 3-5.

MOLDOVEANU, G.A., PAPANGELAKIS, V.G., 2012. *Recovery of rare earth elements adsorbed on clay minerals: I. Desorption mechanism.* Hydrometallurgy. 117, 71-78.

MOLDOVEANU, G.A., PAPANGELAKIS, V.G., 2013. *Recovery of rare earth elements adsorbed on clay minerals: II. Leaching with ammonium sulfate*. Hydrometallurgy. 131, 158-166.

NIU, J.N., QIANG, Y.H., WANG, C.Y., LI, X., ZHOU, Y.H., SHANG, X.Y., ZHUANG, Q.C., 2014. *Nomenclature, structure, morphology and curling mechanism of halloysite.* Acta Mineralogica Sinica. 34, 13-22.

QIU, T.S., QIU, S., WU, H., YAN, H.S., LI, X.B., ZHOU, X.W., 2021. *Adsorption of hydrated $[Y(OH)_2]^+$ on kaolinite (001) surface: Insight from DFT simulation.* Powder Technol. 387, 80-87.

QIU, S., WU, H., YAN, H.S., LI, X.B., QIU, T.S., 2021. *Theoretical investigation of hydrated $[Lu(OH)_2]^+$ adsorption on kaolinite(0 0 1) surface with DFT calculations.* Applied Surface Science, 565, 150473.

QIU, S., QIU, T.S., YAN, H.S., LONG, Q.B., WU, H., LI, X.B., ZHU, D.M., 2022a. *Investigation of protonation and deprotonation processes of kaolinite and its effect on the adsorption stability of rare earth elements*. Colloids and Surfaces A: Physicochemical and Engineering Aspects. 642, 128596.

QIU, S., YAN, H.S., HONG, B.G., LONG, Q.B., XIAO, J., LI, F.J., TONG, L.C., ZHOU, X.W., QIU, T.S., 2022b. *Desorption of REEs from halloysite and illite: A link to the exploitation of ion-adsorption RE ore based on clay species*. Minerals. 12, 1003.

QIU, S., LI, F.J., YAN, H.S., LONG, Q.B., ZHOU, X.W., LI, Y., XIA, Y., 2022c. *Step-Leaching and Pre-Enrichment of Light and Heavy REEs from Kaolinite and Montmorillonite*. ACS Sustainable Chemistry & Engineering, 10(36), 11815-11823.

RAM, R., BECKER, M., BRUGGER, J., ETSCHMANN, B., BURCHER-JONES, C., HOWARD, D., KOOYMAN, P.J., PETERSEN, J., 2019. *Characterisation of a rare earth element- and zirconium-bearing ion-adsorption clay deposit in Madagascar*. Chemical Geology 522, 93-107.

SUN, Y.Y., XU, Q.H., LI, Y.X., 2017. *Leaching kinetics of ion adsorption rare earths using low concentration of ammonium sulfate solution*. Chinese Rare Earths. 38, 61-67.

TERTRE, E., BERGER, G., SIMONI, E., CASTET, S., GIFFAUT, E., LOUBET, M., CATALETTE, H., 2006. *Europium retention onto clay minerals from 25 to 150°C: Experimental measurements, spectroscopic features and sorption modelling*. Geochimica et Cosmochimica Acta 70, 4563-4578.

WANG, C.Q., WANG, H., JIANG, X.Y., HUANG, R., CAO, Y.J., 2019. *Research advances on adsorption of heavy metals by biochar.* Chemical Industry and Engineering Progress. 38, 692-706.

WANG, Z., XIAO, Y.W., FENG, K., 2021. *Metallogenic characteristic and occurrence of REE in ion adsorption type rare earth deposits*. Nonferrous Metals Mieral Processing Section. 6, 43-51.

WEN, T., WANG, G.S., XIE, F.F., LUO, S.H., YIN, S.H., LIU, J., 2022. *Enlightenment of characteristics of La^{3+} adsorption on different rock weathering products on rare earth mineralization*. Chinese Journal of Rare Metals. 46, 1469-1478.

XIAO, Y.F., FENG, Z.Y., HUANG, X.W., HUANG, L., CHEN, Y.Y., WANG, L.S., LONG, Z.Q., 2015. *Recovery of rare earths from weathered crust elution-deposited rare earth ore without ammonia-nitrogen pollution: I. leaching with magnesium sulfate,* Hydrometallurgy. 153, 58-65.

XIAO, Y.F., HUANG, L., LONG, Z.Q., FENG, Z.Y., WANG, L.S., 2016(a). *Adsorption ability of rare earth elements on clay minerals and its practical performance.* Journal of Rare Earths 34, 543-548.

XIAO, Y.F., FENG, Z.Y., HU, G.H., HUANG, L., HUANG, X.W., CHEN, Y.Y., LONG, Z.Q., 2016(b). *Reduction leaching of rare earth from ion-adsorption type rare earths ore with ferrous sulfate*, Journal of Rare Earths. 34,917-923.

XIAO, Y.F., GAO, G.H., HUANG, L., FENG, Z.Y., LAI, F.G., LONG, Z.Q., 2018. *A discussion on the leaching process of the ion-adsorption type rare earth ore with the electrical double layer model*, Minerals Engineering. 120, 35-43.

XIE, G.Y., ZHANG, Y., 2012. *The principle of rare earth luminescent material and the applications*. Piezoelectrics & Acoustooptics. 34, 110-113+117.

XU, C., KYNICKY, J., SMITH, M.P., KOPRIVA, A., BRTNICKY, M., URUBEK, T., YANG, Y.H., ZHAO, Z., HE, CHEN., SONG, W.L., 2017. *Origin of heavy rare earth mineralization in South China*, Nature Communications. 8, 14598.

XU, Q.H., YANG, L.F., ZHANG, L., LI, C.C., WANG, D.S., ZHOU, X.M., ZHOU, X.Z., LI, Y.X. 2018. *Classification and highly efficient leaching of ion adsorption rare earth based on its pH dependence*. Chinese Journal of Inorganic Chemistry. 34, 112-122.

YAN, H.S., YANG, B., ZHOU, X.W., QIU, X.H., ZHU, D.M., WU, H., LI, M.F., LONG, Q.B., XIA, Y., CHEN, J., LI, Y., QIU, T.S., 2022. *Adsorption mechanism of hydrated $Lu(OH)^{2+}$ and $Al(OH)^{2+}$ ions on the surface of kaolinite*. Powder Technology, 407, 117611.

YANG, M.J., LIANG, X.L., MA, L.Y., HUANG, J., HE, H.P., ZHU, J.X., 2019. *Adsorption of REEs on kaolinite and halloysite: A link to the REE distribution on clays in the weathering crust of granite*. Chemical Geology. 525, 210-217.

ZHAI, M.G., WU, F.Y., HU, R.Z., JIANG, S.Y., LI, W.C., WANG, R.C., WANG, D.H., QI, T., QIN, K.Z., WEN, H.J., 2019. *Critical metal mineral resources: current research status and scientifical issues*. Bulletin of National Science Foundation of China. 33, 106-111

ZHOU, F., FENG, J., WU, B.H., ZHANG, Z.Y., WU, X.Y., CHI, R.A., 2018. *Comprehensive chemical experiment of montmorillonite adsorbing rare earth ions*. Experimental Technology and Management. 35, 60-65.

ZHOU, F., HUANG, S.H., LIU, X., FENG, J., LIU, Q., WANG, Z.W., LI, C.C., XU, Y.L., 2021. *Adsorption kinetics and thermodynamics of rare earth on Montmorillonite modified by sulfuric acid.* Colloids and Surfaces A: Physicochemical and Engineering Aspects. 627, 127063.

ZHOU, J.M., LI, M.Y., YUAN, P., LI, Y., LIU, H.M., FAN, W.X., LIU, D., ZHANG, H., 2021. *Partial rehydration of tubular halloysite (7 Å) immersed in $La(NO_3)_3$ solution for 3 years and its implication for understanding REE occurrence in weathered crust elution-deposited rare earth ores*. Applied Clay Science. 213, 106244.

ZHOU, J.M., LIU, H.M., LIU, D., YUAN, P., BU, H.L., DU, P.X., FAN, W.X., LI, M.Y., 2022. *Sorption/desorption of Eu (III) on halloysite and kaolinite.* Applied Clay Science. 216, 106356.